LETTERS

Chiral magnetic order at surfaces driven by inversion asymmetry

M. Bode[1]†, M. Heide[2], K. von Bergmann[1], P. Ferriani[1], S. Heinze[1], G. Bihlmayer[2], A. Kubetzka[1], O. Pietzsch[1], S. Blügel[2] & R. Wiesendanger[1]

Chirality is a fascinating phenomenon that can manifest itself in subtle ways, for example in biochemistry (in the observed single-handedness of biomolecules[1]) and in particle physics (in the charge-parity violation of electroweak interactions[2]). In condensed matter, magnetic materials can also display single-handed, or homochiral, spin structures. This may be caused by the Dzyaloshinskii–Moriya interaction, which arises from spin–orbit scattering of electrons in an inversion-asymmetric crystal field[3,4]. This effect is typically irrelevant in bulk metals as their crystals are inversion symmetric. However, low-dimensional systems lack structural inversion symmetry, so that homochiral spin structures may occur[5]. Here we report the observation of magnetic order of a specific chirality in a single atomic layer of manganese on a tungsten (110) substrate. Spin-polarized scanning tunnelling microscopy reveals that adjacent spins are not perfectly antiferromagnetic but slightly canted, resulting in a spin spiral structure with a period of about 12 nm. We show by quantitative theory that this chiral order is caused by the Dzyaloshinskii–Moriya interaction and leads to a left-rotating spin cycloid. Our findings confirm the significance of this interaction for magnets in reduced dimensions. Chirality in nanoscale magnets may play a crucial role in spintronic devices, where the spin rather than the charge of an electron is used for data transmission and manipulation. For instance, a spin-polarized current flowing through chiral magnetic structures will exert a spin-torque on the magnetic structure[6,7], causing a variety of excitations or manipulations of the magnetization[8,9] and giving rise to microwave emission, magnetization switching, or magnetic motors.

In metallic magnets, itinerant spin-polarized electrons hop across the lattice and exert the Heisenberg exchange interaction[10] between magnetic spin moments **S** located on atomic sites *i* and *j*. As it is a consequence of the Coulomb interaction, the exchange interaction is isotropic. The leading term results in the energy:

$$E_{\mathrm{H}} = \sum_{i,j} J_{ij}\mathbf{S}_i \cdot \mathbf{S}_j \qquad (1)$$

Depending on the signs and values of the exchange constants J_{ij}, equation (1) describes the well-known ferromagnetic or antiferromagnetic phases. The interaction is symmetric—that is, two magnetic configurations with right-handed ($\nwarrow\nearrow$) and left-handed ($\nearrow\nwarrow$) alignment of the magnetic moments have the same energy. During the past 20 years of research, the consensus emerged that this concept scales down to metallic magnets of low dimensions and of nanometre scale, even though the actual values change. For example, owing to the reduced coordination number, the local spin moments of nanomagnets exceed those of bulk magnets. In addition, the magnetic anisotropy, which stabilizes the magnetic order against thermal fluctuations and is responsible for the occurrence of easy and hard axes, increases in structures of reduced dimensions. In nanomagnets, the single-site uniaxial anisotropy is most important, and typically has the form

$$E_{\mathrm{ani}} = \sum_i K_i \sin^2 \varphi_i \qquad (2)$$

described by the anisotropy constant K_i and the angle φ_i between the axis of magnetization and the easy axis at site *i*.

But the fact that nanomagnets frequently lack inversion symmetry (because of the presence of interfaces and surfaces) passed without much attention. Owing to the presence of spin–orbit interaction, which connects the lattice with the spin symmetry, the broken parity of the lattice gives rise to an additional interaction that breaks the inversion invariance of the Heisenberg hamiltonian in equation (1). This is the Dzyaloshinskii–Moriya interaction[3,4], DMI,

$$E_{\mathrm{DM}} = \sum_{i,j} \mathbf{D}_{ij} \cdot \left(\mathbf{S}_i \times \mathbf{S}_j\right) \qquad (3)$$

which arises from spin–orbit scattering of hopping electrons in an inversion asymmetric crystal field ($\mathbf{D}_{ij}$ is the Dzyaloshinskii vector). In such an environment, the scattering sequence of spin-polarized electrons, for example, $i \rightarrow j \rightarrow i$ versus $j \rightarrow i \rightarrow j$, is non-commutative. The presence of the DMI has far-reaching consequences. Depending on the sign, the symmetry properties, and the value of $\mathbf{D}_{ij}$, uniaxial ferro- or antiferromagnetic structures fail to exist and are instead replaced by a directional non-collinear magnetic structure of one specific chirality, $\mathbf{C}_i = \mathbf{S}_i \times \mathbf{S}_{i+1}$, either a right-handed ($C > 0$) or left-handed ($C < 0$) one. In fact, *J*, **D** and *K* span a parameter space containing magnetic structures of unprecedented complexity[11], including two- and three-dimensional cycloidal, helicoidal or toroidal spin structures, or even vortices.

Although chiral magnetic structures have already been observed in reciprocal and real space in bulk samples (see ref. 12 and references therein), we are not aware of any experimental evidence for their existence due to the presence of surfaces or interfaces. To prove the existence, investigate the relevance, and understand the importance of the DMI in nanoscale metals, we revisited the two-dimensional atomic-scale antiferromagnetic (AFM) structure observed within a single layer of manganese atoms on tungsten (110), which has been studied earlier by spin-polarized scanning tunnelling microscopy, SP-STM[13]. We recall that the results were interpreted in terms of an AFM configuration, which consists of a chequerboard arrangement of Mn atoms of antiparallel magnetization. Theoretically determined anisotropy energies indicated that the easy magnetization axis is in-plane along the $[1\bar{1}0]$ direction (Fig. 1a), the surface normal is an intermediate axis, and a hard axis lies along the [001] direction (Fig. 1b).

[1]Institute of Applied Physics and Microstructure Research Center, University of Hamburg, Jungiusstrasse 11, 20355 Hamburg, Germany. [2]Institut für Festkörperforschung, Forschungszentrum Jülich, 52425 Jülich, Germany. †Present address: Center for Nanoscale Materials, Argonne National Laboratory, Argonne, Illinois 60439, USA.

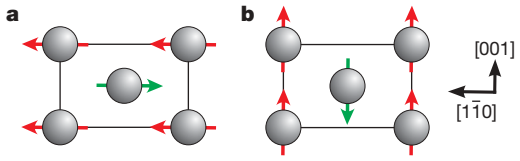

Figure 1 | Antiferromagnetic (AFM) structure of a Mn monolayer on W(110). a, b, Magnetic moments may be oriented along [1$\bar{1}$0] (**a**) and [001] (**b**) directions. According to calculated anisotropy energies ($E_{001} - E_{1\bar{1}0} = 1.6 \pm 0.4$ meV per Mn atom and $E_{110} - E_{1\bar{1}0} = 1.2 \pm 0.4$ meV per Mn atom), the easy and hard axes are along [1$\bar{1}$0] and [001] directions, respectively. The theoretical magnetic moment is $\pm 3.5\mu_B$, where μ_B is the Bohr magneton.

Figure 2a shows the topography of 0.77 atomic layers of Mn grown on a W(110) substrate. The magnetic structure can be imaged directly by SP-STM using magnetically coated W tips. Figure 2b shows a high spatial resolution constant-current image measured on the atomically flat Mn layer using a Cr-coated probe tip sensitive to the in-plane magnetization. The SP-STM data reveal periodic stripes running along the [001] direction, with an inter-stripe distance of 0.47 ± 0.03 nm matching the surface lattice constant along the [1$\bar{1}$0] direction. In an earlier publication[13] this magnetic modulation was interpreted in terms of an in-plane AFM ground state of Mn/W(110). The line section in the lower panel of Fig. 2b reveals, however, that the magnetic amplitude is not constant but modulated with a period of about 6 nm. Further, the magnetic corrugation is not simply a symmetric modulation superimposed on a constant offset I_0 of equation (5) (see Methods). Instead, we find an additional long-wave modulation of I_0 (blue line), which we ascribe to spin–orbit coupling induced variations of the spin-averaged electronic structure[14]. When using in-plane sensitive tips, the minima of the magnetic corrugation are found to coincide with the minima of the long-wave modulation of the spin-averaged local density of states. Within the field of view (Fig. 2b), three antinodes of the magnetic corrugation are visible. Comparing the experimental data with a sine function (red) representing perfect AFM order reveals a phase shift of π between adjacent antinodes.

The long-wavelength modulation of the magnetic amplitude observed in Fig. 2b may be explained by two fundamentally different spin structures: first, a spin-density wave as it occurs, for example, in bulk Cr (ref. 15), or second, a spin spiral. Whereas a spin-density wave is characterized by a sinusoidal modulation of the size of the magnetic moments and the absence of spin rotation, the spin spiral consists of magnetic moments of approximately constant magnitude but whose directions rotate continuously. We denote spin spirals that are confined to a plane perpendicular or parallel to the propagation direction as helical spirals (h-SS) or cycloidal spirals (c-SS), respectively. Figure 2c shows an artist's view of a spin-density wave, a h-SS and a c-SS. According to equation (5) (see Methods), the magnetic contrast vanishes in either case twice over one magnetic period because (1) the sample magnetic moments themselves vanish periodically or (2) the magnetic moments underneath the tip apex are orthogonal with respect to the tip magnetization, $\mathbf{m}_T$. The two cases can, however, be distinguished by addressing different components of the sample magnetization: whereas in case (1) maximum spin contrast is always achieved at lateral positions where the magnetic moments are largest, independent of $\mathbf{m}_T$, in case (2) a rotation of $\mathbf{m}_T$ can shift the position of maximum spin contrast.

Such a rotation of $\mathbf{m}_T$ can be achieved by subjecting an in-plane sensitive Fe-coated tip to an appropriate external magnetic field[16,17] (see sketches in Fig. 3). For samples without a net magnetic moment, it is expected that the sample magnetization remains unaffected. The SP-STM images and line sections of Fig. 3 show data taken at a perpendicular field of $\mu_0 H = 0$ T (Fig. 3a), 1 T (Fig. 3b) and 2 T (Fig. 3c). Using the encircled adsorbate as a marker, we observe maximum magnetic contrast at this lateral position in zero field, indicating large in-plane components of the sample magnetization here. This is also corroborated by the line section, which—in agreement with the in-plane sensitive measurements of Fig. 2b—shows

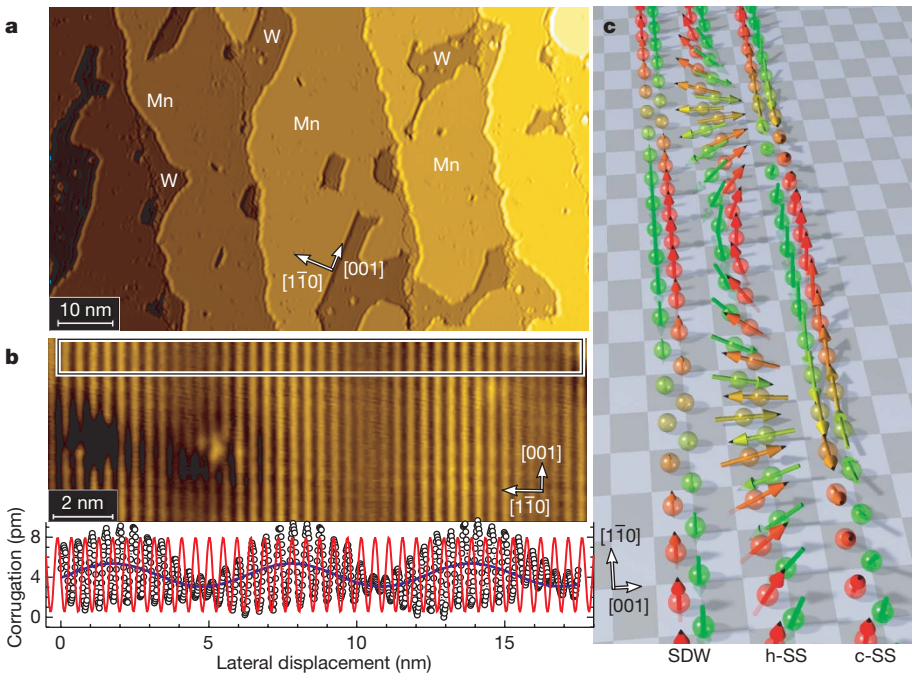

Figure 2 | SP-STM of the Mn monolayer on W(110) and potential spin structures. a, Topography of 0.77 atomic layers of Mn on W(110), **b,** high-resolution constant-current image (upper panel) of the Mn monolayer taken with a Cr-coated tip (tunnelling parameters: $I = 15$ nA, $U = +3$ mV). The stripes along the [001] direction are caused by spin-polarized tunnelling between the magnetic tip and the sample. The averaged line section (lower panel) reveals a magnetic corrugation with a nominal periodicity of 0.448 nm and a long-wavelength modulation. Comparison with a sine wave (red), expected for perfect AFM order, reveals a phase shift of π between adjacent antinodes. In addition, there is an offset modulation (blue line), which we attribute to a varying electronic structure owing to spin–orbit coupling. **c,** Artist's view of the considered spin structures: a spin-density wave (SDW), a helical spin spiral (h-SS) and a left-handed cycloidal spin spiral (c-SS).

high magnetic corrugation at the maximum of the spin-averaged long-wave modulation. With increasing external field, the position of high magnetic corrugation shifts to the left (Fig. 3b) until a node reaches the adsorbate at 2 T (Fig. 3c). The line sections reveal that the magnetic field only shifts the position of high magnetic corrugation but leaves the long-wave spin-averaged modulation unaffected. At 2 T, that is, with an almost perfectly out-of-plane magnetized tip, maximum magnetic contrast is achieved where the spin-averaged signal exhibits a minimum (see line section of Fig. 3c). This observation rules out a spin-density wave, but is a clear proof of a spin spiral with magnetic moments rotating from in-plane (imaged in Fig. 3a) to out-of-plane (imaged in Fig. 3c). Simulations based on a simple SP-STM model[18] (not shown here) indicate that within the signal-to-noise ratio the experimental data are in good agreement with the calculated images for a homogeneously rotating spin spiral. We have performed the same kind of experiment on six separate Mn islands on a different sample (not shown). For each island, we found that the position of maximum magnetic contrast as a function of the external field acting on the tip shifts into the same direction. The

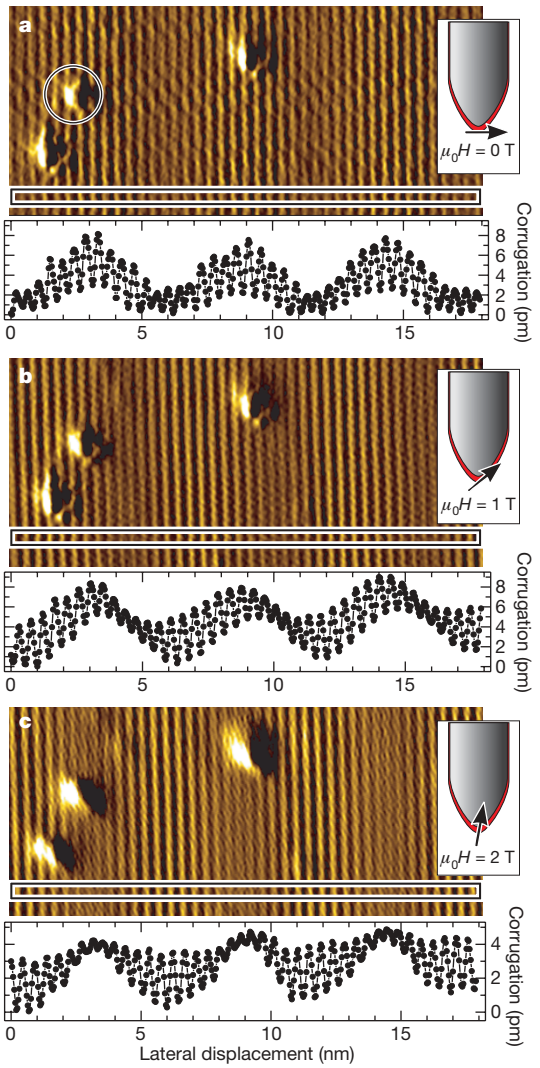

Figure 3 | Field-dependent SP-STM measurements. Magnetically sensitive constant-current images of the Mn monolayer on W(110) (top panels) and corresponding line sections (bottom panels) taken with a ferromagnetic Fe-coated tip at external fields of 0 T (**a**), 1 T (**b**) and 2 T (**c**). As sketched in the insets, the external field rotates the tip magnetization from in-plane (**a**) to out-of-plane (**c**), shifting the position of maximum spin contrast. This proves that the Mn layer does not exhibit a spin-density wave but rather a spin spiral rotating in a plane orthogonal to the surface. (Tunnelling parameters: $I = 2$ nA, $U = 30$ mV.)

statistical probability of this result is only 3%. This suggests that the islands exhibit a spin spiral of only one chirality, as expected for a Dzyaloshinskii–Moriya-driven magnetic configuration. As we cannot control the azimuthal orientation of the tip magnetization, however, we are not able to test experimentally whether the observed spin spiral is helical or cycloidal.

On theoretical grounds, the magnetic ground-state structure minimizes the energy $E = E_{\mathrm{H}} + E_{\mathrm{DM}} + E_{\mathrm{ani}}$. The DMI is a consequence of the spin–orbit coupling. This relativistic effect is weak as compared to the isotropic exchange, and can thus induce only small deviations from the local collinear structure. This allows us to summarize the contributions of the exchange constants J_{ij} and $\mathbf{D}_{ij}$ in terms of an effective spin stiffness J and Dzyaloshinskii vector $\mathbf{D}$ (compare, for example, ref. 19). For a propagation direction along a high symmetry line of the (110) surface, we can apply the symmetry conditions given in ref. 4 and deduce that $\mathbf{D}$ points in-plane and normal to the propagation direction. As E_{DM} favours a chirality $\mathbf{C}_i = \mathbf{S}_i \times \mathbf{S}_{i+1}$ antiparallel to $\mathbf{D}$ and vanishes for $\mathbf{C} \perp \mathbf{D}$, we expect a c-SS and can rule out a h-SS (compare Fig. 2c). Assuming a cycloidal spiral, we can replace $\mathbf{D}$ by a scalar quantity D describing the size and sign of $\mathbf{D}$.

At first, we assume, consistent with our experimental data, a constant canting angle between the moments $\mathbf{S}_i$, $\mathbf{S}_{i+1}$ of two adjacent lattice sites. For such a homogeneous cycloidal spiral, the energy E as function of λ simplifies to

$$E_{\mathrm{cs}}(\lambda) = J\lambda^{-2} + D\lambda^{-1} + \bar{K} \qquad (4)$$

where $|\lambda|$ denotes the cycloidal period length and the sign of λ depends on the chirality, that is, on the rotational direction of the spin spiral. $\bar{K}$ is the anisotropy energy per atom averaged over the spiral. Note that the Dzyaloshinskii–Moriya term is linear in $1/\lambda$, thus the sign of D determines the sign of λ_0 and thus the chirality. The energy $E_{\mathrm{cs}}(\lambda_0)$ of the optimal homogeneous spiral, $\lambda_0 = -2\,J/D$, is lower than the AFM state if the DMI overcomes the average energy penalty per atom for spins spiralling in a plane rather than pointing along a preferred easy axis of magnetization—that is, if $D^2 > 4\,J\,\bar{K}$.

Next, we determine the relevant energy terms for one atomic layer of Mn on W(110) directly from the quantum theory of interacting electrons by applying density functional theory (see Methods)[20]. If we exclude spin–orbit interaction from the calculation (blue crosses in Fig. 4)—that is, considering only isotropic exchange—the total energy minimum occurs for the AFM state ($\lambda_0 = \pm\infty$). Including spin–orbit coupling (red filled circles) has two effects. First, it shifts the energy at the AFM state by the average magnetic anisotropy energy $\bar{K}$. (Note that $\bar{K}$ of the investigated cycloidal spirals amounts to $\bar{K} = \frac{1}{2}(E_{110} - E_{1\bar{1}0}) = 0.6$ meV per Mn atom if the spiral propagates in the $[1\bar{1}0]$ direction and to 1.4 meV per Mn atom if the spiral propagates in the [001] direction.) However, the spin–orbit interaction in surfaces also breaks the inversion symmetry between right- and left-handed spin rotation, and leads to a DMI that contributes a linear term in λ^{-1} to the total energy. As a result, the energy minimum now appears for a left-handed (cycloidal) spin spiral along the $[1\bar{1}0]$ direction with a pitch of $|\lambda_0| = 8$ nm. (Owing to the larger average anisotropy, a spin spiral along the [001] direction (Fig. 4 lower panel) is energetically unfavourable.)

We further investigate inhomogeneous and three-dimensional spirals using more sophisticated micromagnetic models[19], applying the corresponding model parameters (for example, J, D) obtained from fits to the energies of the homogeneous spirals. These calculations confirm that the energy is indeed minimized by a cycloidal spiral. The optimal period deviates only marginally from the period λ_0 of the homogeneous spiral. Keeping in mind that an STM image of a cycloidal modulation of an atomic scale AFM structure repeats twice across a period (compare Fig. 2c), the distance between nodes of the corrugation amplitude in an STM image is calculated to be $\frac{1}{2}|\lambda_0| \approx 4.0$ nm, which is in reasonable agreement with the experimentally observed value of 6 nm.

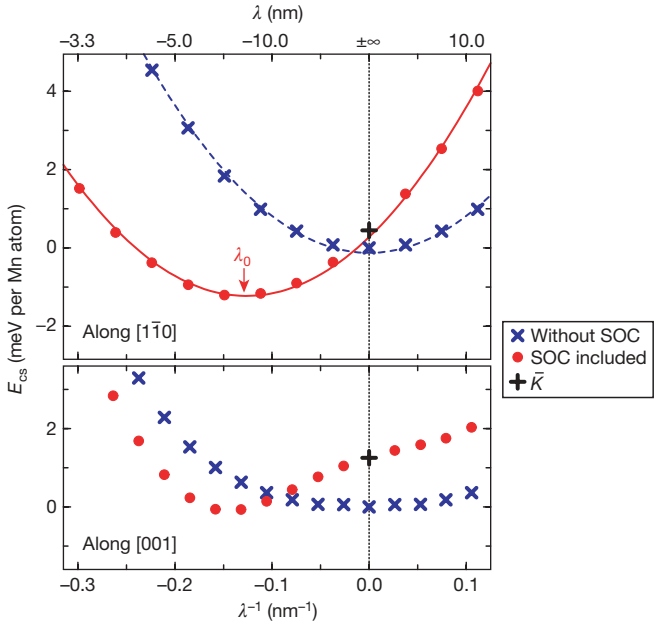

Figure 4 | Calculated energy of homogeneous cycloidal spin spirals. Energy differences for spirals propagating along the two high-symmetry directions [1$\bar{1}$0] (upper panel) and [001] (lower panel) and the c(2 × 2) AFM state as function of the period length, $|\lambda|$. Origin of energy is the AFM state. The minus sign of λ indicates a spiral with left-handed chirality. The data points show the density functional theory results obtained without (blue crosses) and with (red dots) spin–orbit coupling (SOC) included. Broken ($D = \bar{K} = 0$) and solid lines are fits to equation (4) with parameters $J = 94.2\,\mathrm{nm}^2$ meV per Mn atom and $D = 23.8$ nm meV per Mn atom. Note that the possible energy gain is much larger for propagation along the [1$\bar{1}$0] direction than along the [001] direction.

Our finding represents a major extension of the experimentally accessible non-collinear spin structures in thin films, so far not attainable by neutron or magnetic X-ray scattering techniques. In this work, antisymmetric Dzyaloshinskii–Moriya exchange is established as an essential interaction in low-dimensional systems that lack inversion symmetry (such as thin films, surfaces, clusters and atomic wires), and is found able to compete on the same footing with symmetric Heisenberg exchange and magnetic anisotropy to create complex magnetic structures. Our work also changes the perception of magnetic structures in nanomagnets. As the Dzyaloshinskii–Moriya interaction selects magnetic structures of specific chirality, such structures could become useful in the context of spintronics, as they would enable interaction with a spin-current.

METHODS

The SP-STM experiments were performed in an ultrahigh-vacuum system with four separate chambers containing a cryogenic STM ($T = 13 \pm 1$ K). Details of the experimental set-up and the measurement procedures can be found in refs 21 and 22, respectively. Sample preparation procedures are described in ref. 23. All STM images are recorded in the constant-current mode. Spin-integrated measurements are performed with W tips. For spin-resolved measurements, we used Cr- and Fe-covered W tips. When using spin-polarized tips, the tunnelling current I becomes sensitive to the relative magnetic orientation of tip and sample[22,24]

$$I = I_0 + I_{SP}\mathbf{m}_T \cdot \mathbf{m}_S \qquad (5)$$

where the first and second term represent the non-polarized and the spin-polarized part of the tunnelling current, respectively, and $\mathbf{m}_T$ and $\mathbf{m}_S$ are the unit vectors of tip and sample magnetization. In the constant-current mode, the contribution of the spin-polarized part of the tunnelling current, I_{SP}, has been shown to allow atomic-scale imaging of magnetic nanostructures[13,17,24,25].

For theoretical investigations, we used density functional theory[20], which is 'first principles' in that it requires no experimental input other than the nuclear charges. We apply the generalized gradient approximation[26] to the exchange correlation potential and use the full-potential linearized augmented plane wave method. We are able to deal with long-period magnetic structures using the generalized Bloch theorem for homogeneous spirals in combination with a perturbative treatment of the spin–orbit coupling[27]. No sensitivity of our results was found with respect to our choice of computational parameters.

Received 21 December 2006; accepted 30 March 2007.

1. Siegel, J. S. Single-handed cooperation. *Nature* **409,** 777–778 (2001).
2. Ellis, J. Antimatter matters. *Nature* **424,** 631–634 (2003).
3. Dzialoshinskii, I. E. Thermodynamic theory of "weak" ferromagnetism in antiferromagnetic substances. *Sov. Phys. JETP* **5,** 1259–1262 (1957).
4. Moriya, T. Anisotropic superexchange interaction and weak ferromagnetism. *Phys. Rev.* **120,** 91–98 (1960).
5. Fert, A. Magnetic and transport properties of metallic multilayers. *Mater. Sci. Forum* **59&60,** 439–443 (1990).
6. Berger, L. Emission of spin waves by a magnetic multilayer traversed by a current. *Phys. Rev. B* **54,** 9353–9358 (1996).
7. Slonczewski, J. C. Current-driven excitation of magnetic multilayers. *J. Magn. Magn. Mater.* **199,** L1–L11 (1996).
8. Kiselev, S. I. *et al.* Microwave oscillations of a nanomagnet driven by a spin-polarized current. *Nature* **425,** 380–383 (2003).
9. Krivorotov, I. N. *et al.* Time-domain measurements of nanomagnet dynamics driven by spin-transfer torques. *Science* **307,** 228–231 (2005).
10. Heisenberg, W. Zur Theorie des Ferromagnetismus. *Z. Phys.* **49,** 619–636 (1928).
11. Rößler, U. K., Bogdanov, A. N. & Pfleiderer, C. Spontaneous skyrmion ground states in magnetic metals. *Nature* **442,** 797–801 (2006).
12. Uchida, M., Onose, Y., Matsui, Y. & Tokura, Y. Real-space observation of helical spin order. *Science* **311,** 359–361 (2006).
13. Heinze, S. *et al.* Real-space imaging of two-dimensional antiferromagnetism on the atomic scale. *Science* **288,** 1805–1808 (2000).
14. Bode, M. *et al.* Magnetization-direction–dependent local electronic structure probed by scanning tunneling spectroscopy. *Phys. Rev. Lett.* **89,** 237205 (2002).
15. Fawcett, E. Spin-density-wave antiferromagnetism in chromium. *Rev. Mod. Phys.* **60,** 209–283 (1988).
16. Kubetzka, A. *et al.* Revealing antiferromagnetic order of the Fe monolayer on W(001): Spin-polarized scanning tunneling microscopy and first-principles calculations. *Phys. Rev. Lett.* **94,** 087204 (2005).
17. Bode, M. *et al.* Atomic spin structure of antiferromagnetic domain walls. *Nature Mater.* **5,** 477–481 (2006).
18. Heinze, S. Simulation of spin-polarized scanning tunneling microscopy images of nanoscale non-collinear magnetic structures. *Appl. Phys. A* **85,** 407–414 (2006).
19. Dzyaloshinskiĭ, I. E. Theory of helicoidal structures in antiferromagnets III. *Sov. Phys. JETP* **20,** 665–668 (1965).
20. Hohenberg, P. & Kohn, W. Inhomogeneous electron gas. *Phys. Rev.* **136,** B864–B871 (1964).
21. Pietzsch, O. *et al.* A low-temperature ultra-high vacuum scanning tunneling microscope with a split-coil magnet and a rotary motion stepper motor for high spatial resolution studies of surface magnetism. *Rev. Sci. Instrum.* **71,** 424–430 (2000).
22. Bode, M. Spin-polarized scanning tunneling microscopy. *Rep. Prog. Phys.* **66,** 523–581 (2003).
23. Bode, M. *et al.* Structural, electronic, and magnetic properties of a Mn monolayer on W(110). *Phys. Rev. B* **66,** 014425 (2002).
24. Wortmann, D. *et al.* Resolving complex atomic-scale spin structures by spin-polarized scanning tunneling microscopy. *Phys. Rev. Lett.* **86,** 4132–4135 (2001).
25. Yang, H., Smith, A. R., Prikhodko, M. & Lambrecht, W. R. L. Atomic-scale spin-polarized scanning tunneling microscopy applied to Mn_3N_2(010). *Phys. Rev. Lett.* **89,** 226101 (2002).
26. Perdew, J. P., Burke, K. & Ernzerhof, M. Generalized gradient approximation made simple. *Phys. Rev. Lett.* **77,** 3865–3868 (1996).
27. Heide, M. *Magnetic Domain Walls in Ultrathin Films: Contribution of the Dzyaloshinskii-Moriya Interaction.* PhD thesis, RWTH-Aachen (2006).

Acknowledgements Financial support from the project 'spin–orbit effects in magnetic systems' and the Sonderforschungsbereich "Magnetismus vom Einzelatom zur Nanostruktur" of the Deutsche Forschungsgemeinschaft, from the Stifterverband für die Deutsche Wissenschaft, and from the Interdisciplinary Nanoscience Center Hamburg is gratefully acknowledged.

Author Information Reprints and permissions information is available at www.nature.com/reprints. The authors declare no competing financial interests. Correspondence and requests for materials should be addressed to M.B. (mbode@anl.gov).